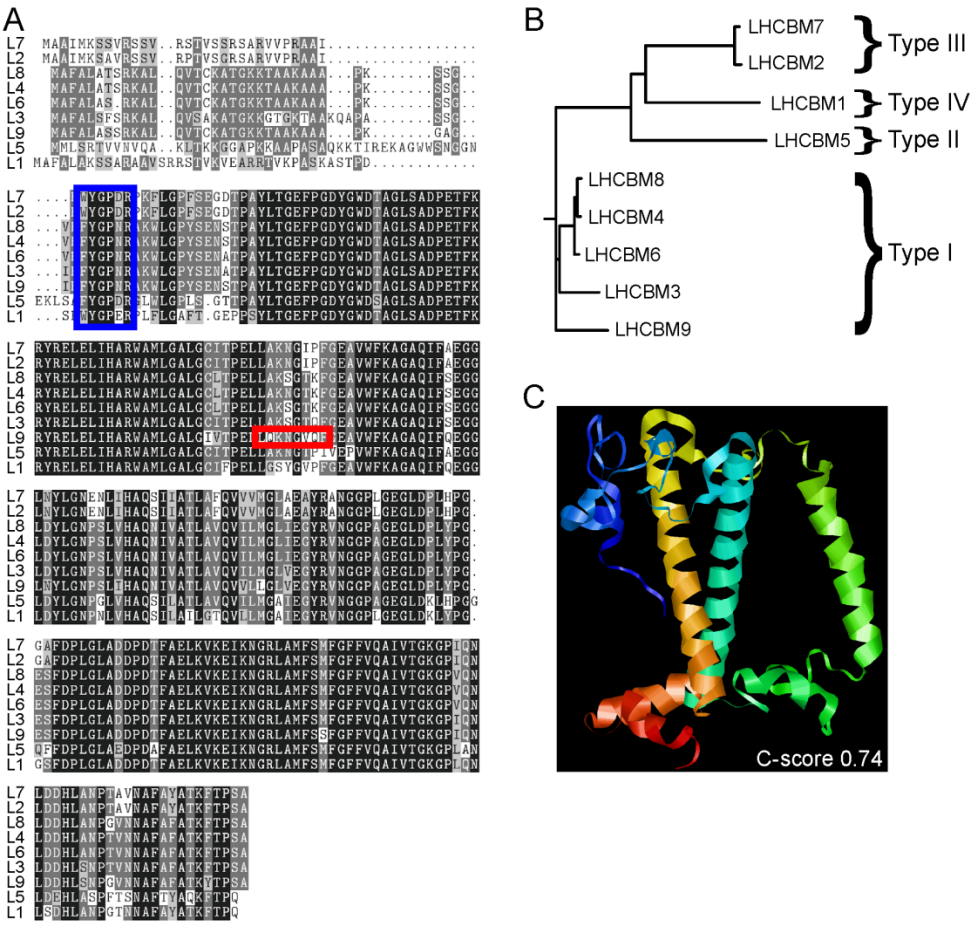

Supplemental Figure 1. Sequence alignment, phylogenic tree and I-Tasser (Roy et al., 2010) model of LHCBM9.

(A) Clustal W multiple sequence alignment of *Chlamydomonas* LHCII proteins. Blue box indicates region of potential trimerization motif, red box indicates specific epitope used for LHCBM9 antibody generation. The alignment was performed via the Biology WorkBench V3.2 platform (http://workbench.sdsc.edu), CLUSTALW – Multiple Sequence Alignment option with default settings.
(B) Rooted phylogenetic tree of LHCBM1-9 and assignment to type I-IV. The tree was generated via the Biology WorkBench V3.2 platform, DRAWGRAM – Draw Rooted Phylogenetic Tree from Alignment option with default settings.
(C) Model of the putative mature LHCBM9 protein (I-TASSER, confidence score indicated) of 238 amino acids and 25.4 kDa.

Roy, A., Kucukural, A., and Zhang, Y. (2010). I-TASSER: a unified platform for automated protein structure and function prediction. Nat. Protoc. **5:** 725-738.

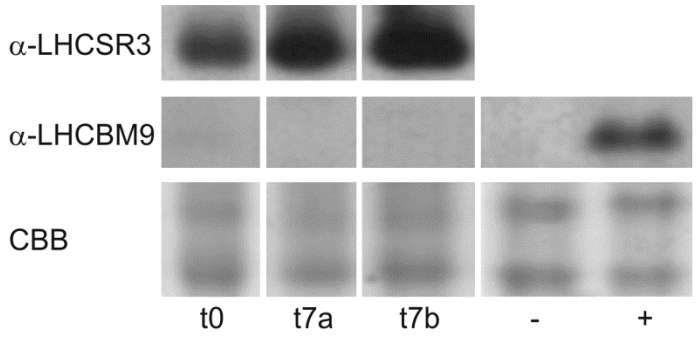

Supplemental Figure 2. Expression pattern of LHCSR3 and LHCBM9 after high light cultivation.

PCS cells were cultivated in photoautotrophic conditions at 1.500 µmol•m^{-2}•s^{-1} for seven hours and immunoblot analysis performed with antibodies specific for LHCSR3 or LHCBM9. Two biological replicates are shown (7a and 7b) and equal amounts of proteins from a sulfur deprivation approach served as controls (- t0; + 24 hours -S). Coomassie Brilliant Blue (CBB) stained SDS-PAGE gel represents the protein loading control.

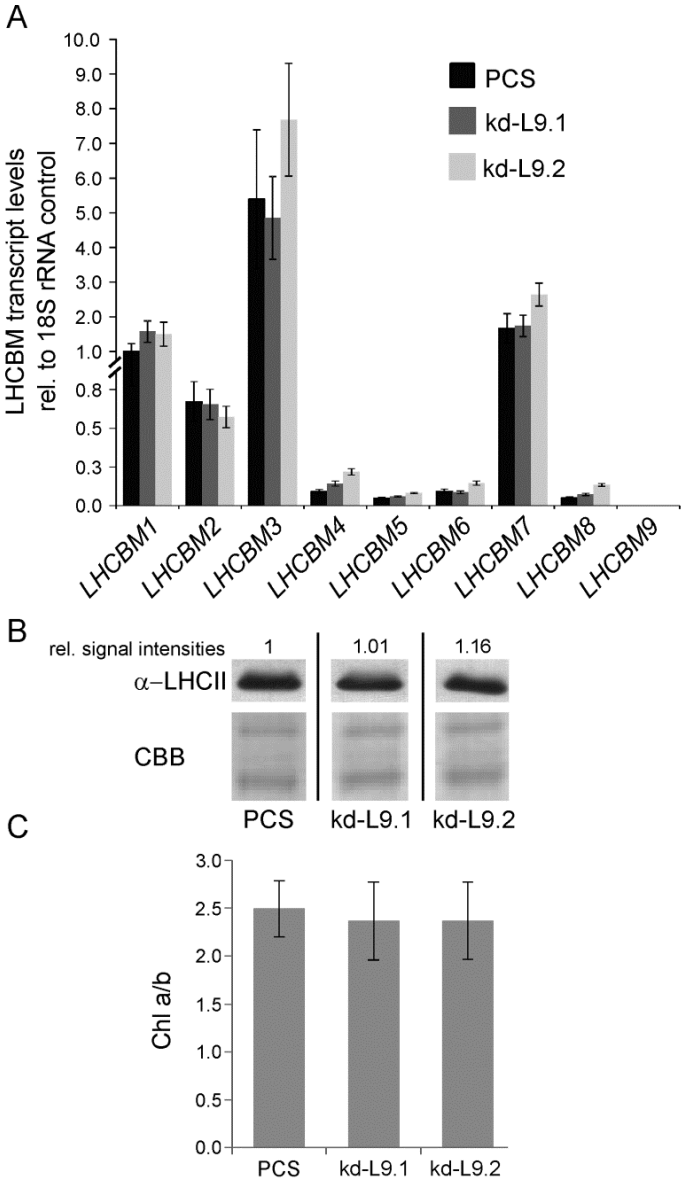

Supplemental Figure 3. Phenotypic characterization of the LHCBM9 knockdown lines kd-L9.1 and kd-L9.2 with respect to the parental control strain (PCS) in nutrient replete conditions.

(A) Quantitative real-time RT-PCR (RT-Q-PCR) analyses of *LHCBM* transcript levels, quantified relative to the mRNA level of the housekeeping gene *18S rRNA*. The mean value for *LHCBM1* for PCS was set to 1.0 and the other values were adjusted accordingly. Error bars represent standard deviation (n=4).
(B) LHCII protein amount as determined with a LHCII-specific antibody (Hippler et al., 2001). Relative signal intensities were quantified with the software GelAnalyzer 2010 (gelanalyzer.com) and are indicated. Coomassie Brilliant Blue (CBB) stained SDS-PAGE gels demonstrate equal protein loading.
(C) Representation of the respective chlorophyll a/b ratios. Error bars represent standard deviation (n=10). No statistical differences in the data were observed (Kruskal-Wallis test, p=0.6232).

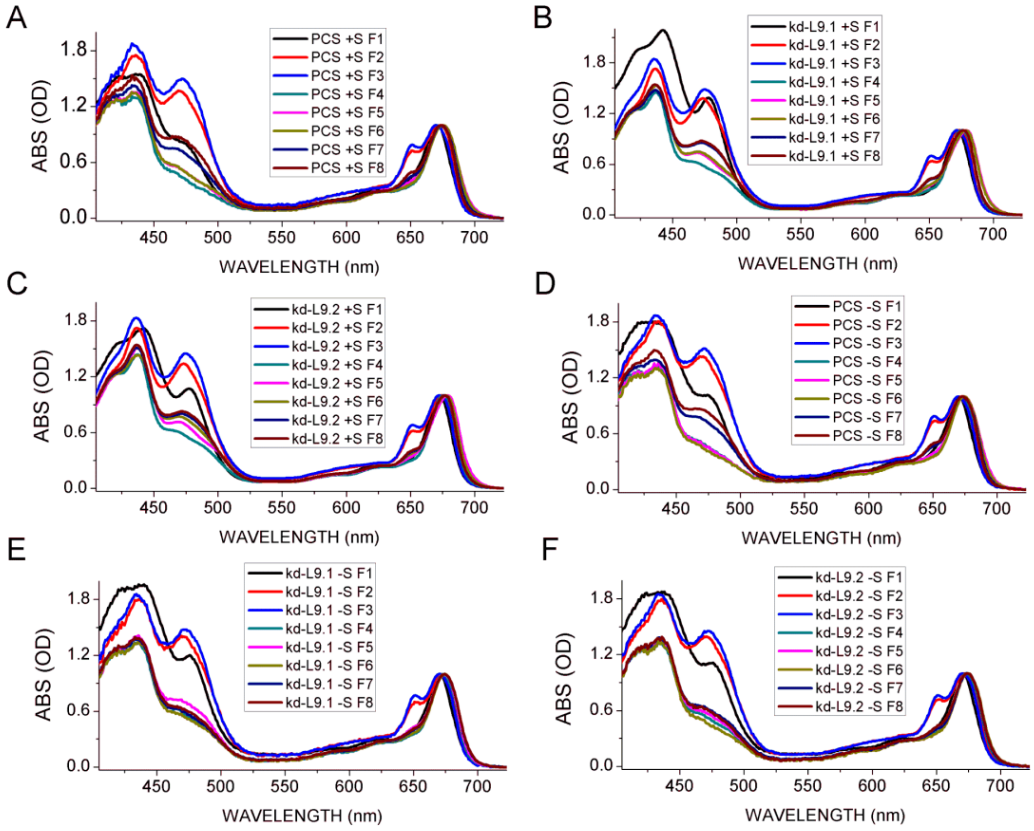

Supplemental Figure 4. Absorption spectra of sucrose gradient fractions.

Fraction recovered from sucrose gradients reported in Figure 3 were analyzed for their absorption spectra in the 400-700 nm spectral range. Absorption spectra were reported for fraction F1-F8 for the different samples in control conditions (+S) or in sulfur deficiency (-S). Each absorption spectrum was normalized to its maximum absorption peak in the Qy region.

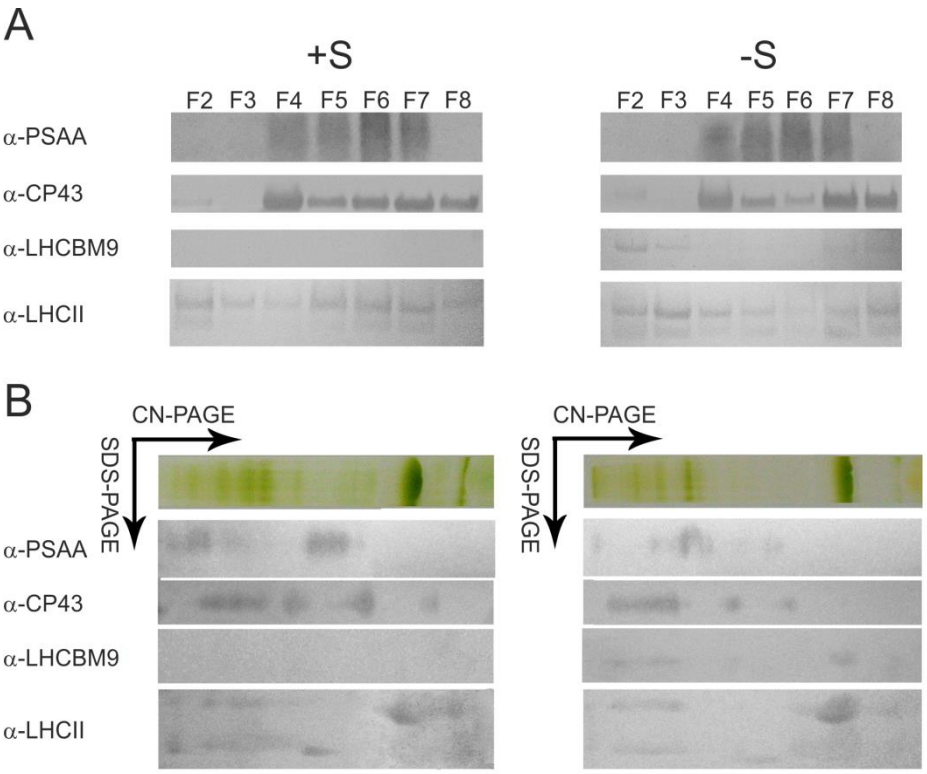

Supplemental Figure 5. Analysis of interactions between LHCBM9 and reaction center complexes by 2-D electrophoresis and immunoblotting.

(A) Immunoblot analysis of fractions from sucrose gradients (shown in Figure 3A) using antibodies recognizing PSAA, CP43, LHCBM9 and LHCII. To allow more distinct LHC signal detections, fractions were loaded at 2.5 µg (fractions F2 and F3) or 5 µg (fractions F4 - 8) of chlorophylls, depending on whether the fractions contained mainly LHC proteins (F2-3) or contained core complexes as well (F4-8).
(B) Two dimensional separation of thylakoid supercomplexes by Clear-Native PAGE (first dimension), followed by denaturing SDS-PAGE and immunoblot detection with PSAA, CP43, LHCBM9 and LHCII antibodies.

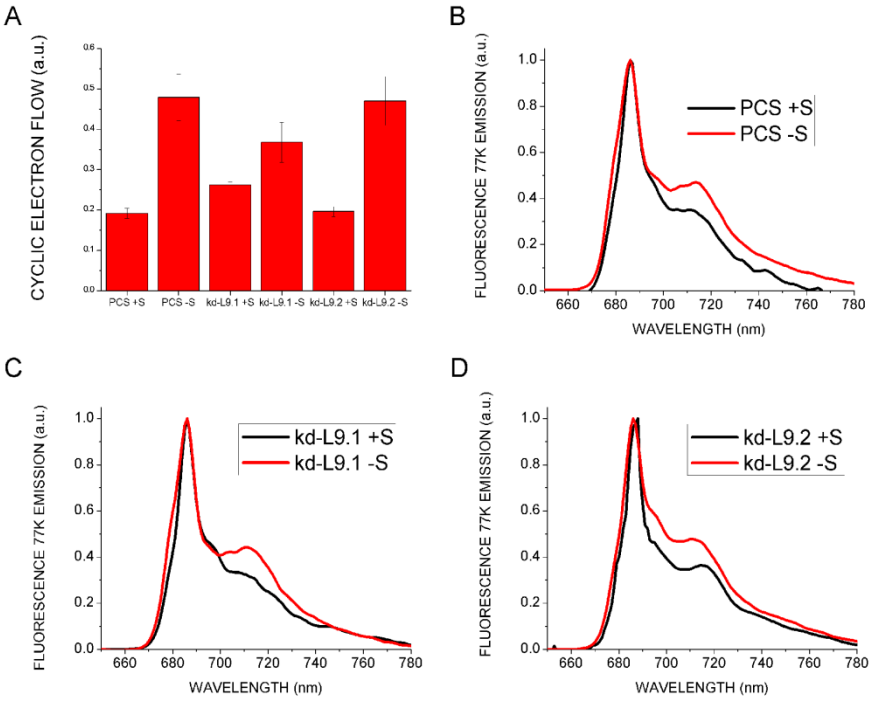

Supplemental Figure 6. Cyclic electron flow around PSI and LHC state transitions measurements.

(A) Cyclic electron flow around PSI was measured in PCS and the knockdown mutants in control conditions and in sulfur deficiency by determination of the maximum P700 activity in cells induced to state 1 and state 2. The level of cyclic electron flow was calculated as one minus the ratio of the maximum P700 activity in state 2 and state 1. Error bars indicate standard deviation (n=3).
(B-D) State transitions were evaluated measuring the fluorescence emission spectra of whole cells at 77K in control conditions (+S) or in sulfur deficiency (-S).

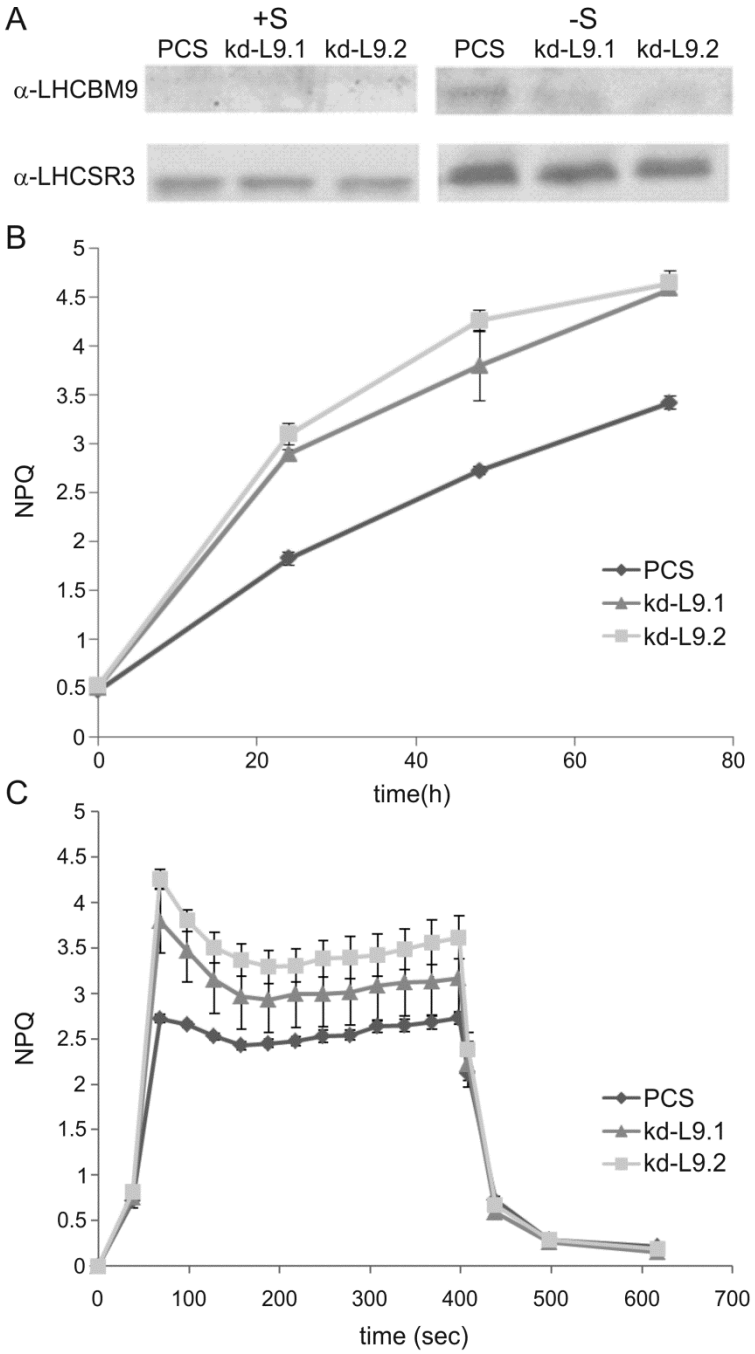

Supplemental Figure 7. LHCBM9 accumulation and NPQ characteristics in high light conditions.

Cells were cultivated in +S medium or in -S medium at 400 µmol•m^{-2}•s^{-1}.
(A) Immunoblot analysis of thylakoids purified from PCS, kd-L9.1 and kd-L9.2 after 48 h of cultivation.
(B) Maximum NPQ values of PCS and the LHCBM9 knockdown lines, determined via PAM fluorometry. The cultivation time (hours) in high light and sulfur deficiency is indicated.
(C) NPQ induction kinetics determined via PAM fluorometry. Cell samples were harvested after 48 h of cultivation in high light and sulfur deficiency. The duration of the NPQ measurement (sec) is indicated.

Supplemental Figure 8. Protein sequence alignment of LHCBM9 with LHCBM1 and LHCII from *Arabidopsis thaliana* (Lhcb1 subunit).

The N-terminal amino acids omitted from the recombinant proteins are indicated in blue. The chlorophyll binding residues (according to the nomenclature from Kuehlbrandt et al., 1994) and the tyrosine residue reported to be critical for neoxanthin binding (N1 (Caffarri et al., 2007)) are indicated in red.

Caffarri, S., Passarini, F., Bassi, R., and Croce, R. (2007). A specific binding site for neoxanthin in the monomeric antenna proteins CP26 and CP29 of Photosystem II. FEBS Lett. **581:** 4704-4710.
Kuehlbrandt, W., Wang, D.N., and Fujiyoshi, Y. (1994). Atomic model of plant light-harvesting complex by electron crystallography. Nature **367:** 614-621.

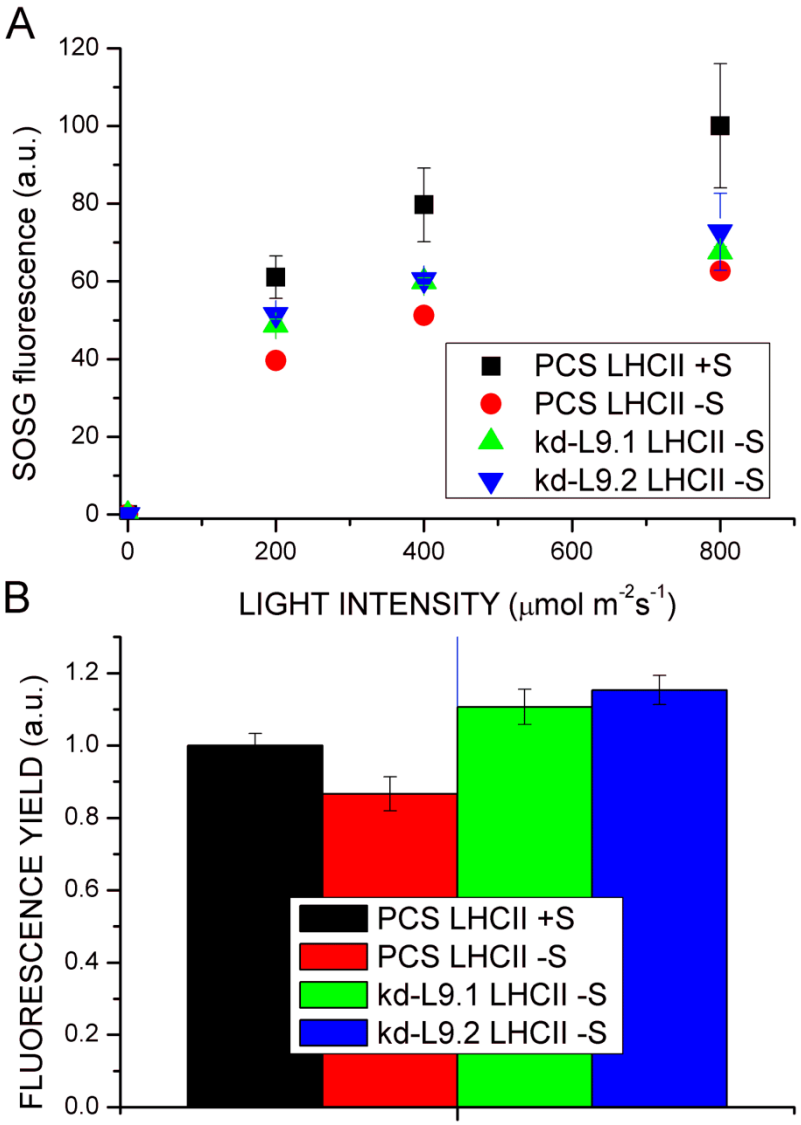

Supplemental Figure 9. Fluorescence quantum yield and singlet oxygen production of native LHCII trimers.

(A) Singlet oxygen production measured in LHCII trimers as the increase of SOSG fluorescence at 530 nm upon illumination at different light intensities.
(B) Relative fluorescence quantum yield of LHCII purified from PCS cells in control condition (+S, black) and from PCS (red) and the knockdown mutant lines (kd-L9.1, green and kd-L9.2, blue) in sulfur deficiency (-S).
Error bars indicate standard deviation (n=5).

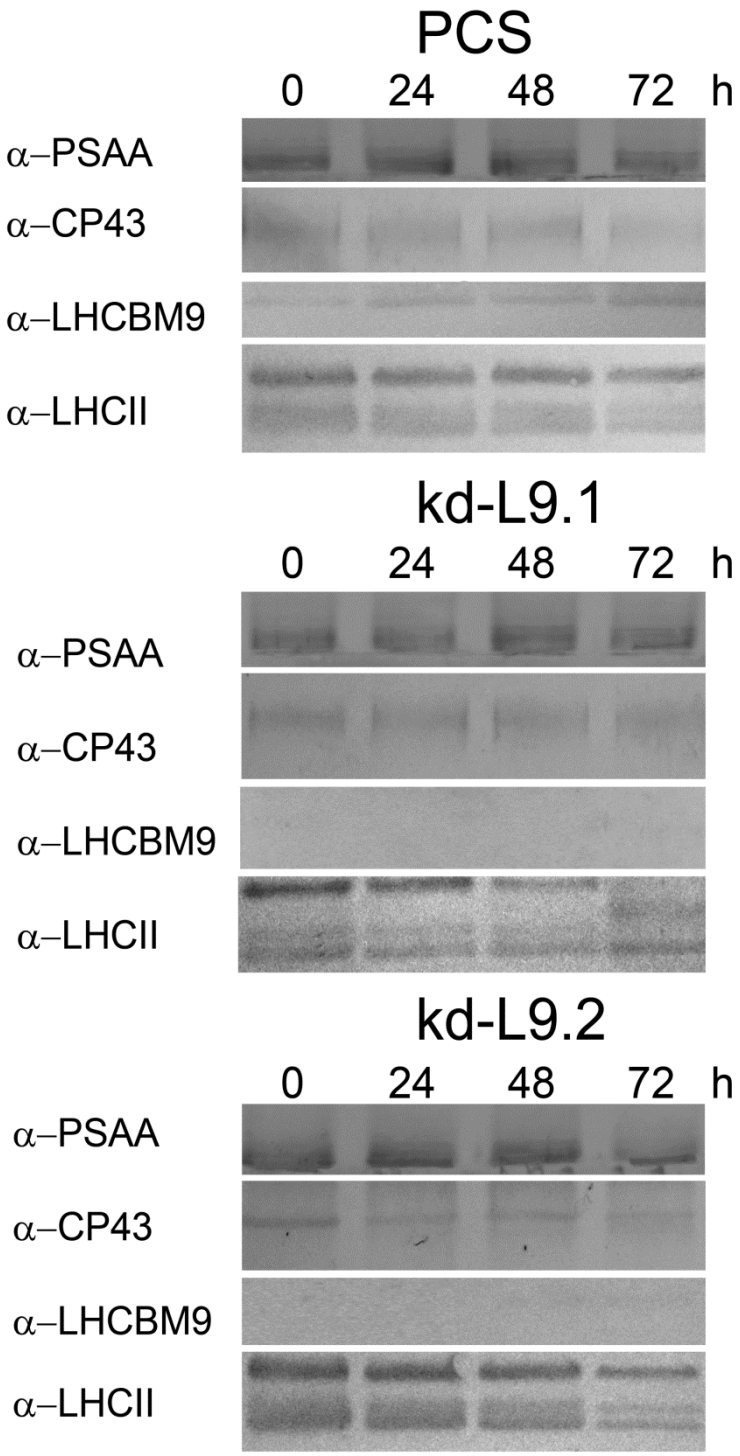

Supplemental Figure 10. Immunoblot analysis of LHCBM protein degradation during sulfur deficiency.

Immunoblot analysis of PSAA, CP43, LHCBM9 and LHCII proteins of PCS, kd-L9.1 and kd-L9.2 mutants during sulfur deficiency (0-72 hours). The antibody used as α-LHCII generally recognize all LHCBM proteins.

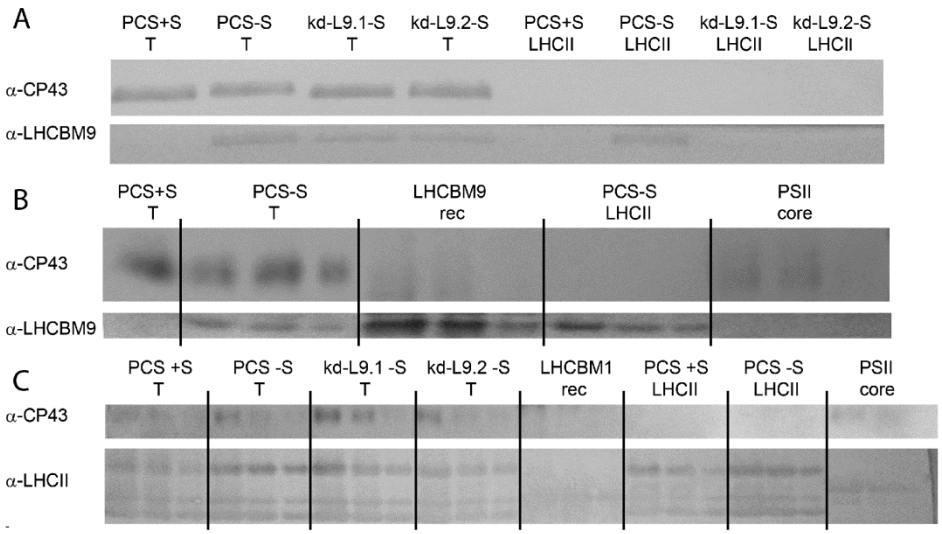

Supplemental Figure 11. Immunoblot analysis of thylakoids and LHCII fractions purified from PCS and kd-L9.1 and kd-L9.2 mutants, and recombinant LHCBM9 and LHCBM1.

(A) Immunoblot analysis with LHCBM9 and CP43 antibodies of thylakoids purified from PCS in control conditions (+S) and from kd-L9.1 and kd-L9.2 in sulfur deficiency for 48 hours (-S). This analysis served as basis to calculate the ratio of LHCBM9 per PSII in PCS and mutants.
(B) Immunoblot analysis with LHCBM9 and CP43 antibodies of PCS thylakoids in -S conditions, recombinant LHCBM9, LHCII trimers isolated from PCS thylakoids in -S conditions and PSII core isolated from PCS in +S conditions. This analysis served as basis to calculate the stoichiometry of LHCBM9 per PSII and per LHCII trimers.
(C) Immunoblot analysis with an antibody generally recognizing LHCII subunits of thylakoids purified from PCS in +S conditions and PCS, kd-L9.1, kd-L9.2 in -S conditions, LHCII trimers purified from PCS in -S conditions and recombinant LHCBM1. This analysis served as basis to calculate the stoichiometry of LHCII and LHCBM1 per PSII.
T: thylakoids, rec: recombinant protein.

Supplemental Table 1. Gene and protein characteristics of LHCBM9 as determined by *in silico* analyses.

LHCBM9 *in silico* analysis		
Accession Numbers	Phytozome NCBI GenBank	Cre06.g284200 XP_001695466
Gene	Number of nucleotides (start to stop codon)	1748 nt
	Number of introns in coding sequence	4
	Intron sizes	128 nt; 329 nt; 269 nt; 257 nt
	Size of the coding sequence (start to stop codon)	765 nt
	Chromosome localization	Chromosome 6
Protein	LHCII-type	I
Unprocessed	Number of amino acids	254 AA
	Calculated molecular weight	27.1 kDa
	Theoretical pI	5.96
Putative mature	Number of amino acids	238 AA
	Calculated molecular weight (kDa)	25.4
	Theoretical pI	5.44

Supplemental Table 2. Pigment analysis of reconstituted Lhcbm proteins.
HPLC anlaysis of pigments extracted from recombinant, refolded LHCBM1, LHCBM2, LHCBM3 and LHCBM9 proteins. Chl, chlorophylls, Chl a, chlorophyll a, Chl b, chlorophyll b, Chl a/b, chlorophyll a/b ratio, Chl/ Car, chlorophyll to carotenoid ratio, Cars, total carotenoids, Neo, neoxanthin, Vio, violaxanthin, Lute, lutein. The numbers for chlorophylls and carotenoids represent the moles of each pigment bound by one mole of apoprotein. Chl a/b and Chl/Car ratios are absolute values.

	Chl	Chla	Chl b	Chl a/b	Chl/car	Cars	Neo	Vio	Lute
LHCBM1	14	8.95	5.05	1.77	4.58	3.05	1.36	0.27	1.42
LHCBM2	14	7.75	6.25	1.24	3.69	3.79	1.38	0.68	1.73
LHCBM3	14	7.76	6.24	1.24	3.88	3.61	1.42	0.52	1.67
LHCBM9	14	8.7	5.3	1.64	4.14	3.38	1.4	0.43	1.56